

Search for Chargino and Neutralino Production at $\sqrt{s} = 189 \text{ GeV}$ at LEP

The OPAL Collaboration

Abstract

A search for charginos and neutralinos, predicted by supersymmetric theories, is performed using a data sample of 182.1 pb^{-1} taken at a centre-of-mass energy of 189 GeV with the OPAL detector at LEP. No evidence for chargino or neutralino production is found. Upper limits on chargino and neutralino pair production ($\tilde{\chi}_1^+ \tilde{\chi}_1^-$, $\tilde{\chi}_1^0 \tilde{\chi}_2^0$) cross-sections are obtained as a function of the chargino mass ($m_{\tilde{\chi}_1^\pm}$), the lightest neutralino mass ($m_{\tilde{\chi}_1^0}$) and the second lightest neutralino mass ($m_{\tilde{\chi}_2^0}$). Within the Constrained Minimal Supersymmetric Standard Model framework, and for $m_{\tilde{\chi}_1^\pm} - m_{\tilde{\chi}_1^0} \geq 5 \text{ GeV}$, the 95% confidence level lower limits on $m_{\tilde{\chi}_1^\pm}$ are 93.6 GeV for $\tan \beta = 1.5$ and 94.1 GeV for $\tan \beta = 35$. These limits are obtained assuming a universal scalar mass $m_0 \geq 500 \text{ GeV}$. The corresponding limits for all m_0 are 78.0 and 71.7 GeV . The 95% confidence level lower limits on the lightest neutralino mass, valid for any value of $\tan \beta$ are 32.8 GeV for $m_0 \geq 500 \text{ GeV}$ and 31.6 GeV for all m_0 .

(Submitted to Phys. Lett. B)

The OPAL Collaboration

G. Abbiendi², K. Ackerstaff⁸, G. Alexander²³, J. Allison¹⁶, K.J. Anderson⁹, S. Anderson¹²,
S. Arcelli¹⁷, S. Asai²⁴, S.F. Ashby¹, D. Axen²⁹, G. Azuelos^{18,a}, A.H. Ball⁸, E. Barberio⁸,
R.J. Barlow¹⁶, J.R. Batley⁵, S. Baumann³, J. Bechtluft¹⁴, T. Behnke²⁷, K.W. Bell²⁰, G. Bella²³,
A. Bellerive⁹, S. Bentvelsen⁸, S. Bethke¹⁴, S. Betts¹⁵, O. Biebel¹⁴, A. Biguzzi⁵, I.J. Bloodworth¹,
P. Bock¹¹, J. Böhme¹⁴, O. Boeriu¹⁰, D. Bonacorsi², M. Boutemeur³³, S. Braibant⁸,
P. Bright-Thomas¹, L. Brigliadori², R.M. Brown²⁰, H.J. Burckhart⁸, P. Capiluppi²,
R.K. Carnegie⁶, A.A. Carter¹³, J.R. Carter⁵, C.Y. Chang¹⁷, D.G. Charlton^{1,b}, D. Chrisman⁴,
C. Ciocca², P.E.L. Clarke¹⁵, E. Clay¹⁵, I. Cohen²³, J.E. Conboy¹⁵, O.C. Cooke⁸, J. Couchman¹⁵,
C. Couyoumtzelis¹³, R.L. Coxe⁹, M. Cuffiani², S. Dado²², G.M. Dallavalle², S. Dallison¹⁶,
R. Davis³⁰, S. De Jong¹², A. de Roeck⁸, P. Dervan¹⁵, K. Desch²⁷, B. Dienes^{32,h}, M.S. Dixit⁷,
M. Donkers⁶, J. Dubbert³³, E. Duchovni²⁶, G. Duckeck³³, I.P. Duerdoth¹⁶, P.G. Estabrooks⁶,
E. Etzion²³, F. Fabbri², A. Fanfani², M. Fanti², A.A. Faust³⁰, L. Feld¹⁰, P. Ferrari¹²,
F. Fiedler²⁷, M. Fierro², I. Fleck¹⁰, A. Frey⁸, A. Fürtjes⁸, D.I. Futyan¹⁶, P. Gagnon⁷,
J.W. Gary⁴, G. Gaycken²⁷, C. Geich-Gimbel³, G. Giacomelli², P. Giacomelli², W.R. Gibson¹³,
D.M. Gingrich^{30,a}, D. Glenzinski⁹, J. Goldberg²², W. Gorn⁴, C. Grandi², K. Graham²⁸,
E. Gross²⁶, J. Grunhaus²³, M. Gruwé²⁷, C. Hajdu³¹, G.G. Hanson¹², M. Hansroul⁸, M. Hapke¹³,
K. Harder²⁷, A. Harel²², C.K. Hargrove⁷, M. Harin-Dirac⁴, M. Hauschild⁸, C.M. Hawkes¹,
R. Hawkings²⁷, R.J. Hemingway⁶, G. Herten¹⁰, R.D. Heuer²⁷, M.D. Hildreth⁸, J.C. Hill⁵,
P.R. Hobson²⁵, A. Hocker⁹, K. Hoffman⁸, R.J. Homer¹, A.K. Honma^{28,a}, D. Horváth^{31,c},
K.R. Hossain³⁰, R. Howard²⁹, P. Hüntemeyer²⁷, P. Igo-Kemenes¹¹, D.C. Imrie²⁵, K. Ishii²⁴,
F.R. Jacob²⁰, A. Jawahery¹⁷, H. Jeremie¹⁸, M. Jimack¹, C.R. Jones⁵, P. Jovanovic¹, T.R. Junk⁶,
N. Kanaya²⁴, J. Kanzaki²⁴, D. Karlen⁶, V. Kartvelishvili¹⁶, K. Kawagoe²⁴, T. Kawamoto²⁴,
P.I. Kayal³⁰, R.K. Keeler²⁸, R.G. Kellogg¹⁷, B.W. Kennedy²⁰, D.H. Kim¹⁹, A. Klier²⁶,
T. Kobayashi²⁴, M. Kobel³, T.P. Kokott³, M. Kolrep¹⁰, S. Komamiya²⁴, R.V. Kowalewski²⁸,
T. Kress⁴, P. Krieger⁶, J. von Krogh¹¹, T. Kuhl³, P. Kyberd¹³, G.D. Lafferty¹⁶, H. Landsman²²,
D. Lanske¹⁴, J. Lauber¹⁵, I. Lawson²⁸, J.G. Layter⁴, D. Lellouch²⁶, J. Letts¹², L. Levinson²⁶,
R. Liebisch¹¹, J. Lillich¹⁰, B. List⁸, C. Littlewood⁵, A.W. Lloyd¹, S.L. Lloyd¹³, F.K. Loebinger¹⁶,
G.D. Long²⁸, M.J. Losty⁷, J. Lu²⁹, J. Ludwig¹⁰, D. Liu¹², A. Macchiolo¹⁸, A. Macpherson³⁰,
W. Mader³, M. Mammelli⁸, S. Marcellini², T.E. Marchant¹⁶, A.J. Martin¹³, J.P. Martin¹⁸,
G. Martinez¹⁷, T. Mashimo²⁴, P. Mättig²⁶, W.J. McDonald³⁰, J. McKenna²⁹, E.A. Mckigney¹⁵,
T.J. McMahon¹, R.A. McPherson²⁸, F. Meijers⁸, P. Mendez-Lorenzo³³, F.S. Merritt⁹, H. Mes⁷,
I. Meyer⁵, A. Michelini², S. Mihara²⁴, G. Mikenberg²⁶, D.J. Miller¹⁵, W. Mohr¹⁰, A. Montanari²,
T. Mori²⁴, K. Nagai⁸, I. Nakamura²⁴, H.A. Neal^{12,f}, R. Nisius⁸, S.W. O’Neale¹, F.G. Oakham⁷,
F. Odoricci², H.O. Ogren¹², A. Okpara¹¹, M.J. Oreglia⁹, S. Orito²⁴, G. Pásztor³¹, J.R. Pater¹⁶,
G.N. Patrick²⁰, J. Patt¹⁰, R. Perez-Ochoa⁸, S. Petzold²⁷, P. Pfeifenschneider¹⁴, J.E. Pilcher⁹,
J. Pinfold³⁰, D.E. Plane⁸, P. Poffenberger²⁸, B. Poli², J. Polok⁸, M. Przybycień^{8,d}, A. Quadt⁸,
C. Rembser⁸, H. Rick⁸, S. Robertson²⁸, S.A. Robins²², N. Rodning³⁰, J.M. Roney²⁸, S. Rosati³,
K. Roscoe¹⁶, A.M. Rossi², Y. Rozen²², K. Runge¹⁰, O. Runolfsson⁸, D.R. Rust¹², K. Sachs¹⁰,
T. Saeki²⁴, O. Sahr³³, W.M. Sang²⁵, E.K.G. Sarkisyan²³, C. Sbarra²⁹, A.D. Schaile³³,
O. Schaile³³, P. Scharff-Hansen⁸, J. Schieck¹¹, S. Schmitt¹¹, A. Schöning⁸, M. Schröder⁸,
M. Schumacher³, C. Schwick⁸, W.G. Scott²⁰, R. Seuster¹⁴, T.G. Shears⁸, B.C. Shen⁴,
C.H. Shepherd-Themistocleous⁵, P. Sherwood¹⁵, G.P. Siroli², A. Skuja¹⁷, A.M. Smith⁸,
G.A. Snow¹⁷, R. Sobie²⁸, S. Söldner-Rembold^{10,e}, S. Spagnolo²⁰, M. Sproston²⁰, A. Stahl³,
K. Stephens¹⁶, K. Stoll¹⁰, D. Strom¹⁹, R. Ströhmer³³, B. Surrow⁸, S.D. Talbot¹, P. Taras¹⁸,
S. Tarem²², R. Teuscher⁹, M. Thiergen¹⁰, J. Thomas¹⁵, M.A. Thomson⁸, E. Torrence⁸,

S. Towers⁶, T. Trefzger³³, I. Trigger¹⁸, Z. Trócsányi^{32,g}, E. Tsur²³, M.F. Turner-Watson¹,
I. Ueda²⁴, R. Van Kooten¹², P. Vannerem¹⁰, M. Verzocchi⁸, H. Voss³, F. Wäckerle¹⁰,
A. Wagner²⁷, D. Waller⁶, C.P. Ward⁵, D.R. Ward⁵, P.M. Watkins¹, A.T. Watson¹,
N.K. Watson¹, P.S. Wells⁸, N. Wermes³, D. Wetterling¹¹, J.S. White⁶, G.W. Wilson¹⁶,
J.A. Wilson¹, T.R. Wyatt¹⁶, S. Yamashita²⁴, V. Zacek¹⁸, D. Zer-Zion⁸

¹School of Physics and Astronomy, University of Birmingham, Birmingham B15 2TT, UK

²Dipartimento di Fisica dell' Università di Bologna and INFN, I-40126 Bologna, Italy

³Physikalisches Institut, Universität Bonn, D-53115 Bonn, Germany

⁴Department of Physics, University of California, Riverside CA 92521, USA

⁵Cavendish Laboratory, Cambridge CB3 0HE, UK

⁶Ottawa-Carleton Institute for Physics, Department of Physics, Carleton University, Ottawa, Ontario K1S 5B6, Canada

⁷Centre for Research in Particle Physics, Carleton University, Ottawa, Ontario K1S 5B6, Canada

⁸CERN, European Organisation for Particle Physics, CH-1211 Geneva 23, Switzerland

⁹Enrico Fermi Institute and Department of Physics, University of Chicago, Chicago IL 60637, USA

¹⁰Fakultät für Physik, Albert Ludwigs Universität, D-79104 Freiburg, Germany

¹¹Physikalisches Institut, Universität Heidelberg, D-69120 Heidelberg, Germany

¹²Indiana University, Department of Physics, Swain Hall West 117, Bloomington IN 47405, USA

¹³Queen Mary and Westfield College, University of London, London E1 4NS, UK

¹⁴Technische Hochschule Aachen, III Physikalisches Institut, Sommerfeldstrasse 26-28, D-52056 Aachen, Germany

¹⁵University College London, London WC1E 6BT, UK

¹⁶Department of Physics, Schuster Laboratory, The University, Manchester M13 9PL, UK

¹⁷Department of Physics, University of Maryland, College Park, MD 20742, USA

¹⁸Laboratoire de Physique Nucléaire, Université de Montréal, Montréal, Quebec H3C 3J7, Canada

¹⁹University of Oregon, Department of Physics, Eugene OR 97403, USA

²⁰CLRC Rutherford Appleton Laboratory, Chilton, Didcot, Oxfordshire OX11 0QX, UK

²²Department of Physics, Technion-Israel Institute of Technology, Haifa 32000, Israel

²³Department of Physics and Astronomy, Tel Aviv University, Tel Aviv 69978, Israel

²⁴International Centre for Elementary Particle Physics and Department of Physics, University of Tokyo, Tokyo 113-0033, and Kobe University, Kobe 657-8501, Japan

²⁵Institute of Physical and Environmental Sciences, Brunel University, Uxbridge, Middlesex UB8 3PH, UK

²⁶Particle Physics Department, Weizmann Institute of Science, Rehovot 76100, Israel

²⁷Universität Hamburg/DESY, II Institut für Experimental Physik, Notkestrasse 85, D-22607 Hamburg, Germany

²⁸University of Victoria, Department of Physics, P O Box 3055, Victoria BC V8W 3P6, Canada

²⁹University of British Columbia, Department of Physics, Vancouver BC V6T 1Z1, Canada

³⁰University of Alberta, Department of Physics, Edmonton AB T6G 2J1, Canada

³¹Research Institute for Particle and Nuclear Physics, H-1525 Budapest, P O Box 49, Hungary

³²Institute of Nuclear Research, H-4001 Debrecen, P O Box 51, Hungary

³³Ludwigs-Maximilians-Universität München, Sektion Physik, Am Coulombwall 1, D-85748 Garching, Germany

^a and at TRIUMF, Vancouver, Canada V6T 2A3

^b and Royal Society University Research Fellow

^c and Institute of Nuclear Research, Debrecen, Hungary

^d and University of Mining and Metallurgy, Cracow

^e and Heisenberg Fellow

^f now at Yale University, Dept of Physics, New Haven, USA

^g and Department of Experimental Physics, Lajos Kossuth University, Debrecen, Hungary.

1 Introduction

Supersymmetric (SUSY) extensions of the Standard Model predict the existence of charginos and neutralinos [1]. Charginos, $\tilde{\chi}_i^\pm$, are the mass eigenstates formed by the mixing of the fields of the fermionic partners of the charged gauge bosons (winos) and those of the charged Higgs bosons (charged higgsinos). Fermionic partners of the γ , the Z boson, and the neutral Higgs bosons mix to form the mass eigenstates called neutralinos, $\tilde{\chi}_j^0$ ¹. If charginos exist and are sufficiently light, they are pair-produced at LEP through γ - or Z-exchange in the s -channel. For the wino component, there is an additional production process through scalar electron-neutrino ($\tilde{\nu}_e$) exchange in the t -channel. The production cross-section is large (several pb) unless the scalar neutrino (sneutrino) is light, in which case the cross-section is reduced by destructive interference between the s -channel and t -channel diagrams [2]. In much of the parameter space, $\tilde{\chi}_1^+$ decays dominantly into $\tilde{\chi}_1^0\ell^+\nu$ or $\tilde{\chi}_1^0q\bar{q}'$ via a virtual W boson. For small scalar lepton masses, decays to leptons via a scalar lepton become important. R-parity conservation is assumed throughout this note. With this assumption, the $\tilde{\chi}_1^0$ is stable and invisible² and the experimental signature for $\tilde{\chi}_1^+\tilde{\chi}_1^-$ events is large missing momentum transverse to the beam axis.

Neutralino pairs ($\tilde{\chi}_1^0\tilde{\chi}_2^0$) can be produced through a virtual Z or γ (s -channel) or by a scalar electron (t -channel) exchange [4]. The $\tilde{\chi}_2^0$ will decay into $\tilde{\chi}_1^0\nu\bar{\nu}$, $\tilde{\chi}_1^0\ell^+\ell^-$ or $\tilde{\chi}_1^0q\bar{q}$ through a virtual Z boson, sneutrino, slepton, squark or a neutral SUSY Higgs boson (h^0 or A^0). The decay via a virtual Z is the dominant mode in most of the parameter space. For small scalar lepton masses, decays to a lepton pair via a scalar lepton are important. The experimental signature of $\tilde{\chi}_1^0\tilde{\chi}_2^0$ events is an acoplanar pair of leptons or jets. If the mass difference between $\tilde{\chi}_2^0$ and $\tilde{\chi}_1^0$ is small, the experimental signature becomes monojet-like.

Motivated by Grand Unification and to simplify the physics interpretation, the Constrained Minimal Supersymmetric Standard Model (Constrained MSSM) [1, 5] is used to guide the analysis but the results are also applied to more general models. At the grand unified (GUT) mass scale, in the Constrained MSSM all the gauginos are assumed to have a common mass, $m_{1/2}$, and all the sfermions have a common mass, m_0 . Details are given in Section 5.2.

Previous searches for charginos and neutralinos have been performed using data collected near the Z peak (LEP1), at centre-of-mass energies (\sqrt{s}) of 130–136 GeV [6], 161 GeV [7], 170–172 GeV [8,9], and 183 GeV [10,11], with luminosities of about 100, 5, 10, 10 and 60 pb⁻¹ respectively. No evidence for signal has been found.

In 1998 the LEP e^+e^- collider at CERN was operated at $\sqrt{s}=188.6$ GeV. This paper reports on direct searches for charginos and neutralinos performed using the data sample collected at this centre-of-mass energy. The total integrated luminosity collected with the OPAL detector at this energy is 182.1 pb⁻¹. The selection criteria are similar to those used in [10], but have been modified to improve the sensitivity of the analysis at the current energy. The description of the OPAL detector and its performance can be found in Ref. [12] and [13].

¹In each case, the index $i = 1, 2$ or $j = 1$ to 4 is ordered by increasing mass.

²The lightest supersymmetric particle (LSP) is either $\tilde{\chi}_1^0$ or the scalar neutrino. We assume $\tilde{\chi}_1^0$ is the LSP in the direct searches described in this paper. If the scalar neutrino is lighter than the chargino, $\tilde{\chi}_1^+ \rightarrow \tilde{\nu}\ell^+$ becomes the dominant decay mode. For this case, we use the results of Ref. [3] to calculate limits, as mentioned in Section 5.2.

2 Event Simulation

Chargino and neutralino signal events are generated with the DFGT generator [14] which includes spin correlations and allows for a proper treatment of both the W boson and the Z boson width effects in the chargino and heavy neutralino decays. The generator includes initial-state radiation and uses the JETSET 7.4 package [15] for the hadronisation of the quark-antiquark system in the hadronic decays of charginos and neutralinos. SUSYGEN [16] is used to calculate the branching fractions for the Constrained MSSM interpretation of the analysis.

The sources of background to the chargino and neutralino signals are two-photon, lepton pair, multihadronic and four-fermion processes. Two-photon processes are the most important background for the case of a small mass difference between the $\tilde{\chi}_1^\pm$ and the $\tilde{\chi}_1^0$, or between the $\tilde{\chi}_2^0$ and the $\tilde{\chi}_1^0$, since such events have small visible energy and small transverse momentum. Using the Monte Carlo generators PHOJET [17], PYTHIA [15] and HERWIG [18], hadronic events from two-photon processes are simulated in which the invariant mass of the photon-photon system is larger than 5.0 GeV. Monte Carlo samples for four-lepton events ($e^+e^-e^+e^-$, $e^+e^-\mu^+\mu^-$ and $e^+e^-\tau^+\tau^-$) are generated with the Vermaseren program [19]. All other four-fermion processes except for regions of phase-space covered by the two-photon simulations, are simulated using the grc4f generator [20], which takes into account all interferences. The dominant contributions come from W^+W^- , $W e \nu$, $\gamma^* Z^{(*)}$ and $ZZ^{(*)}$ processes. Lepton pairs are generated using the KORALZ [21] generator for $\tau^+\tau^-(\gamma)$ and $\mu^+\mu^-(\gamma)$ events, and the BHWIDE [22] program for $e^+e^- \rightarrow e^+e^-(\gamma)$ events. Multihadronic ($q\bar{q}(\gamma)$) events are simulated using PYTHIA [15].

Generated signal and background events are processed through the full simulation of the OPAL detector [23] and the same event analysis chain is applied to the simulated events as to the data.

3 Analysis

Calculations of experimental variables are performed as in [8]. The following preselections are applied to reduce background due to two-photon events and interactions of beam particles with the beam pipe or residual gas: (1) the number of charged tracks is required to be at least two; (2) the observed transverse momentum of the whole event is required to be larger than 1.8 GeV; (3) the energy deposited in each silicon-tungsten forward calorimeter and in each forward detector has to be less than 2 GeV (these detectors are located in the forward region, with polar angle ³ $|\cos\theta| > 0.99$, surrounding the beam pipe); (4) the visible invariant mass of the event has to exceed 2 GeV; (5) there should be no signal in the MIP plug scintillators ⁴.

³A right-handed coordinate system is adopted, where the x -axis points to the centre of the LEP ring, and positive z is along the electron beam direction. The angles θ and ϕ are the polar and azimuthal angles, respectively.

⁴The MIP plug scintillators [13] are an array of thin scintillating tiles with embedded wavelength shifting fibre readout which have been installed to improve the hermiticity of the detector. They cover the polar angular range between 43 and 200 mrad.

3.1 Detection of charginos

The event sample is divided into three mutually exclusive categories, motivated by the topologies expected for chargino events. Separate analyses are applied to the preselected events in each category:

- (A) $N_{\text{ch}} > 4$ and no isolated leptons, where N_{ch} is the number of charged tracks. The isolated lepton selection criteria are the same as those described in Ref. [10]. When both $\tilde{\chi}_1^+$ and $\tilde{\chi}_1^-$ decay hadronically, signal events tend to fall into this category for all but the smallest values of $\Delta M_+ (\equiv m_{\tilde{\chi}_1^+} - m_{\tilde{\chi}_1^0})$.
- (B) $N_{\text{ch}} > 4$ and at least one isolated lepton. If just one of the $\tilde{\chi}_1^\pm$ decays leptonically, signal events tend to fall into this category.
- (C) $N_{\text{ch}} \leq 4$. Events tend to fall into this category if ΔM_+ is small or if both charginos decay leptonically.

The fraction of $\tilde{\chi}_1^+ \tilde{\chi}_1^-$ events falling into category (A) is about 35-50% for most of the ΔM_+ range. This fraction drops to less than 15% if ΔM_+ is smaller than 5 GeV, since the average charged track multiplicity of the events becomes small. Similarly, the fraction of events falling into category (B) is also about 35-50% for most of the ΔM_+ range and is less than 10% if ΔM_+ is smaller than 5 GeV. In contrast, when ΔM_+ is smaller than 10 GeV, the fraction of events falling into category (C) is greater than about 50%, while if ΔM_+ is larger than 20 GeV, this fraction is about 10%.

Since the chargino event topology mainly depends on the difference between the chargino mass and the lightest neutralino mass, different selection criteria are applied to four ΔM_+ regions: (I) $\Delta M_+ \leq 10$ GeV, (II) $10 \text{ GeV} < \Delta M_+ \leq m_{\tilde{\chi}_1^+}/2$, (III) $m_{\tilde{\chi}_1^+}/2 < \Delta M_+ \leq m_{\tilde{\chi}_1^+} - 20$ GeV, and (IV) $m_{\tilde{\chi}_1^+} - 20 \text{ GeV} < \Delta M_+ \leq m_{\tilde{\chi}_1^+}$. In region (I), background events come mainly from the two-photon processes. In regions (II) and (III), the main background processes are the four-fermion processes (W^+W^- , single W and $\gamma^*Z^{(*)}$). In these two regions the background level is modest. In region (IV) the W^+W^- background becomes large and dominant. Since the W^+W^- background is significant in the region of $\Delta M_+ > 85$ GeV where the chargino decays via an on-mass-shell W-boson, a special analysis is applied to improve the sensitivity to the chargino signal for $m_{\tilde{\chi}_1^+} > 85$ GeV and $\Delta M_+ \gtrsim 85$ GeV. Overlap between this analysis and the region (IV) standard analysis is avoided by selecting the analysis which minimises the expected cross-section limit calculated with only the expected number of background events.

For each region a single set of cut values is determined which minimises the expected limit on the signal cross-section at 95% confidence level (C.L.) using the method of Ref. [24]. In this procedure, only the expected number of background events is taken into account and therefore the choice of cuts is independent of the number of candidates actually observed.

The variables used in the selection criteria and their cut values are optimised in each ΔM_+ region. They are identical to the ones of Ref. [10] unless otherwise stated, and are therefore only briefly described in the following sections.

3.1.1 Analysis (A) ($N_{\text{ch}} > 4$ without isolated leptons)

After the preselection, cuts on $E_{\text{fwd}}/E_{\text{vis}}$, $|\cos\theta_{\text{miss}}|$, $|P_z|$ and $|P_z|/E_{\text{vis}}$, are applied to further reduce background events from the two-photon and multihadronic processes. E_{vis} is the total visible energy of the event, E_{fwd} is the visible energy in the region of $|\cos\theta| > 0.9$, θ_{miss} is the polar angle of the missing momentum and P_z is the visible momentum along the beam axis. In regions (III) and (IV), the cut values for $E_{\text{fwd}}/E_{\text{vis}}$ and $|\cos\theta_{\text{miss}}|$ have been changed with respect to Ref. [10], requiring them to be smaller than 0.15 and 0.90 respectively. Most of the two-photon background events are rejected by cuts against small P_t^{HCAL} and P_t , the transverse momentum of the event measured with and without using the hadron calorimeter, respectively. In region (I), a cut is also applied against large P_t^{HCAL} ($P_t^{\text{HCAL}} \leq 30$ GeV) to reduce the W^+W^- background.

Jets are reconstructed using the Durham algorithm [25] with jet resolution parameter $y_{\text{cut}} = 0.005$. By requiring the number of jets (N_{jet}) to be between 3 and 5 inclusive, monojet events from the process $\gamma^*Z^{(*)} \rightarrow q\bar{q}\nu\bar{\nu}$ are rejected for regions (I) and (II), and background events from $q\bar{q}(\gamma)$ and $W\nu$ processes are reduced in regions (III) and (IV).

In order to determine the acoplanarity angle ⁵ (ϕ_{acop}), events passing the selection described above are forced into two jets, again using the Durham algorithm. Each jet is required to be far from the beam axis by cutting on its polar angle θ_j ($j=1,2$). This cut ensures a good measurement of ϕ_{acop} and further reduces the background from $q\bar{q}(\gamma)$ and two-photon processes. The acoplanarity angle is required to be larger than 15° to reduce the $q\bar{q}(\gamma)$ background. The acoplanarity angle distribution for region (III) is shown in Figure 1(a) before this cut.

The cut on the visible mass, M_{vis} , is optimised for each ΔM_+ region. If a lepton candidate (ℓ') is found with an algorithm based on the ‘‘looser’’ isolation condition described in Ref. [8], the energy of this lepton, $E_{\ell'}$, and the invariant mass calculated without this lepton, $M_{\text{had}'}$, must be different from the values expected for $W^+W^- \rightarrow \ell\nu q\bar{q}'$ events. The cuts on $E_{\ell'}$ and $M_{\text{had}'}$ have been optimized with respect to Ref. [10]: for region (I) no cut is applied; for region (III) $M_{\text{had}'}$ is required to be smaller than 65 GeV and $E_{\ell'}$ smaller than 25 GeV.

The background from W^+W^- events and single- W events is efficiently suppressed by requiring that the highest and second highest jet energies, E_1 and E_2 , be smaller than the typical jet energy expected for the $W^+W^- \rightarrow 4$ -jet process. The cuts on E_1 and E_2 are identical to the ones in Ref. [10] apart from region (II) where E_1 is required to be between 2 and 30 GeV. In addition, in regions (III) and (IV), if E_1 is larger than 40 GeV, M_{vis} is required to be either smaller than 70 GeV or larger than 95 GeV. In regions (III) and (IV) three-jet events with $|P_z| < 10$ GeV are also rejected if M_{vis} is close to the W mass. These cuts reduce the $W^+W^- \rightarrow \tau\nu q\bar{q}'$ background with low-energy decay products of the τ .

A special analysis is applied in the region of $\Delta M_+ \gtrsim 85$ GeV, since the event topology of the signal is very similar to that of $W^+W^- \rightarrow 4$ jets. After selecting well contained events with the cuts $|\cos\theta_{\text{miss}}| < 0.95$, $E_{\text{fwd}}/E_{\text{vis}} < 0.15$ and $|P_z| < 30$ GeV, multi-jet events with large visible energy are selected with $N_{\text{jet}} \geq 4$ and $110 < E_{\text{vis}} < 170$ GeV. To select a clear 4-jet topology $y_{34} \geq 0.0075$, $y_{23} \geq 0.04$ and $y_{45} \leq 0.0015$ are also required, where $y_{\{n\}\{n+1\}}$ is defined as the minimum y_{cut} value at which the reconstruction of the event switches from $n+1$ to n jets. Events having a ‘‘jet’’ consisting of a single γ with energy greater than 20 GeV are considered to be $\gamma q\bar{q}g$ and are rejected.

⁵The acoplanarity angle, ϕ_{acop} , is defined as $180^\circ - \phi$, where ϕ is the opening angle in the (r, ϕ) plane between the two jets.

The numbers of observed events and background events expected from the four different sources, for each ΔM_+ region and for the special analysis, are given in Table 1. Typical detection efficiencies for $\tilde{\chi}_1^+ \tilde{\chi}_1^-$ events are 20–65% for $\Delta M_+ = 10\text{--}80$ GeV in the standard analysis, and 20–30% for $m_{\tilde{\chi}_1^+} \geq 85$ GeV and $\Delta M_+ \geq 85$ GeV.

Region	I $\Delta M_+ \leq 10$ GeV	II $10 \text{ GeV} < \Delta M_+$ $\leq m_{\tilde{\chi}_1^+}/2$	III $m_{\tilde{\chi}_1^+}/2 < \Delta M_+$ $\leq m_{\tilde{\chi}_1^+} - 20$ GeV	IV $m_{\tilde{\chi}_1^+} - 20$ GeV $< \Delta M_+ \leq m_{\tilde{\chi}_1^+}$	special $\Delta M_+ \geq 85$ GeV
background					
$\gamma\gamma$	0.93	0.46	0.46	0.46	0.00
$\ell^+ \ell^- (\gamma)$	0.00	0.00	0.02	0.02	0.00
$q\bar{q} (\gamma)$	0.07	0.22	0.83	1.83	4.57
4f	0.55	1.27	16.54	24.66	23.09
total bkg	1.5 ± 0.7	2.0 ± 0.5	17.8 ± 0.9	27.0 ± 1.1	27.7 ± 1.0
observed	2	3	22	29	31

Table 1: The numbers of expected background events for various Standard Model processes, normalised to the integrated luminosity, and the number of observed events in each ΔM_+ region and for the special analysis for category (A). The errors in the total background include only the statistical error of the Monte Carlo samples.

3.1.2 Analysis (B) ($N_{\text{ch}} > 4$ with isolated leptons)

After the preselection, cuts on $|\cos \theta_{\text{miss}}|$ and $E_{\text{fwd}}/E_{\text{vis}}$ are applied to reject two-photon background events. The cut on $E_{\text{fwd}}/E_{\text{vis}}$ has been tightened with respect to Ref. [10]: it is required to be smaller than 0.15 in regions (I) and (II) and smaller than 0.2 in regions (III) and (IV).

In order to reject the $W^+W^- \rightarrow \ell\nu q\bar{q}'$ background, the following cuts are applied: the momentum of isolated lepton candidates should be smaller than that expected from decays of the W (smaller than 15 GeV, 30 GeV, 40 GeV and between 5 and 40 GeV for regions (I) to (IV) respectively) and the invariant mass (M_{had}) of the event calculated excluding the highest momentum isolated lepton is required to be smaller than the W mass (smaller than 20 GeV and 40 GeV for regions (I) and (II), between 10 and 60 GeV for region (III), and between 15 and 70 GeV for region (IV)). The distribution of M_{had} after the ϕ_{acop} cut is shown in Figure 1(b) for region (III). As is evident in this figure, most of the W^+W^- background events are rejected by this cut. The invariant mass of the system formed by the missing momentum and the most energetic isolated lepton, $M_{\ell\text{miss}}$, is required to be larger than 110 GeV for region (IV). Finally, a M_{vis} cut is applied to reject $W e \nu$ events in which a fake lepton candidate is found in the $W \rightarrow q\bar{q}'(g)$ decay: it is required to be smaller than 30 GeV for region (I), between 25 and 85 GeV for region (III), and no requirement on M_{vis} is applied for region (IV).

A special analysis is applied in the region of $\Delta M_+ \gtrsim 85$ GeV where there is a large W^+W^- background. The selection criteria are identical to those in region (IV) up to the ϕ_{acop} cut. To reject further $W^+W^- \rightarrow \ell\nu q\bar{q}'$ events while keeping a good signal efficiency, M_{had} is required to be between 70 and 95 GeV, M_{vis} between 90 and 125 GeV, and $M_{\ell\text{miss}}$ between 90 and 130 GeV.

The numbers of observed events and background events expected from the four different sources, for each ΔM_+ region and for the special analysis, are given in Table 2. Typical detection

efficiencies for $\tilde{\chi}_1^+ \tilde{\chi}_1^-$ events are 40–65% for $\Delta M_+ = 10\text{--}80$ GeV for the standard analysis, and 20–30% for $m_{\tilde{\chi}_1^+} \geq 85$ GeV and $\Delta M_+ \geq 85$ GeV.

Region	I $\Delta M_+ \leq 10$ GeV	II $10 \text{ GeV} < \Delta M_+$ $\leq m_{\tilde{\chi}_1^+}/2$	III $m_{\tilde{\chi}_1^+}/2 < \Delta M_+$ $\leq m_{\tilde{\chi}_1^+} - 20$ GeV	IV $m_{\tilde{\chi}_1^+} - 20$ GeV $< \Delta M_+ \leq m_{\tilde{\chi}_1^+}$	special $\Delta M_+ \geq 85$ GeV
background					
$\gamma\gamma$	3.80	0.46	0.00	0.00	0.00
$\ell^+ \ell^- (\gamma)$	0.02	0.04	0.11	0.05	0.02
$q\bar{q} (\gamma)$	0.00	0.11	0.14	0.11	0.04
4f	0.62	1.38	4.30	6.37	23.45
total bkg	4.4 ± 1.3	2.0 ± 0.5	4.6 ± 0.4	6.5 ± 0.5	23.5 ± 0.9
observed	2	1	4	7	27

Table 2: The numbers of expected background events for various Standard Model processes, normalised to the integrated luminosity, and the number of observed events in each ΔM_+ region and for the special analysis for category (B). The errors in the total background include only the statistical error of the Monte Carlo samples.

3.1.3 Analysis (C) ($N_{\text{ch}} \leq 4$)

This analysis is especially important for the region of $\Delta M_+ \leq 5$ GeV. Because the background varies significantly with ΔM_+ in region (I), this region is split into 2 sub-regions (a,b).

In order to reject events with charged particles which escape detection in the main detector, the net charge of the event is required to be zero. Since the signal is expected to have a two-lepton or two-jet topology, events are forced into two jets using the Durham jet algorithm [25]. To improve the jet assignment, each jet must contain at least one charged track ($N_{\text{ch},j} \geq 1$), must have significant energy ($E_j > 1.5$ GeV) and the magnitude of the sum of the track charges ($|Q_j|$) must not exceed 1. The P_t/E_b distributions for region (III) are shown in Figure 1(c) after these cuts. In region (I), if the acoplanarity angle is smaller than 70° , cuts are applied on P_t , a_t (the transverse momentum perpendicular to the event thrust axis), and $|\cos \theta_a|$, where $\theta_a \equiv \tan^{-1}(a_t/P_z)$. These cuts reduce the background contamination from two-photon and $\tau^+ \tau^-$ processes. They are identical to those in Ref. [10] for region (Ib) but have been further optimized for region (Ia) where a_t/E_{beam} is required to lie between 0.025 and 0.1 and $|\cos \theta_a|$ to be smaller than 0.9. To further reduce the two-photon background, cuts on P_t and $|\cos \theta_{\text{miss}}|$ are applied in region (I) if the acoplanarity angle is larger than 70° and in all other regions for any value of acoplanarity angle. The cuts on $|\cos \theta_{\text{miss}}|$ are identical to those in Ref. [10] apart from region (Ia) where it is required to be smaller than 0.75. P_t/E_{beam} should be between 0.02 and 0.04, between 0.03 and 0.05, and between 0.035 and 0.075 for regions (Ia), (Ib) and (II), and should be larger than 0.095 and 0.1 for regions (III) and (IV).

To reduce the background from $e^+ e^- \mu^+ \mu^-$ events in which one of the muons is emitted at a small polar angle and is not reconstructed as a good track, events are rejected if there is a track segment in the muon chamber or a hadron calorimeter cluster at a small polar angle, and within 1 radian in (r, ϕ) of the missing momentum direction (\vec{P}_{miss}).

Cuts on $|\cos\theta_j|$ and ϕ_{acop} are applied to reject two-photon, lepton-pair and $\gamma^*Z^{(*)} \rightarrow \ell^+\ell^-\nu\bar{\nu}$ events. The values of these cuts have been slightly modified with respect to Ref. [10] in that $|\cos\theta_j|$ is now required to be smaller than 0.75 in region (Ia), and ϕ_{acop} should lie between 50° and 160° for region (Ia) and between 20° and 160° for region (Ib). $W^+W^- \rightarrow \ell^+\nu\ell^-\bar{\nu}$ events are rejected by upper cuts on M_{vis} (20 GeV, 25 GeV, 30 GeV, 50 GeV and 75 GeV for regions (Ia) to (IV)) and on the higher energy of the two jets, E_1/E_{beam} (identical to Ref. [10] apart from region (Ia) where it is required to be smaller than 0.2).

The numbers of background events expected from the four different sources, for each ΔM_+ region, are given in Table 3. The typical detection efficiencies for $\tilde{\chi}_1^+\tilde{\chi}_1^-$ events are 30–65% for $\Delta M_+ \gtrsim 10$ GeV, and the modest efficiency of 20% is obtained for $\Delta M_+ = 5$ GeV.

Region	I		II	III	IV
Sub-Region	a	b	$10 \text{ GeV} < \Delta M_+$	$m_{\tilde{\chi}_1^+}/2 < \Delta M_+$	$m_{\tilde{\chi}_1^+} - 20 \text{ GeV} < \Delta M_+$
	$3 \leq \Delta M_+ \leq 5 \text{ GeV}$	$5 < \Delta M_+ \leq 10 \text{ GeV}$	$\leq m_{\tilde{\chi}_1^+}/2$	$\leq m_{\tilde{\chi}_1^+} - 20 \text{ GeV}$	$\leq m_{\tilde{\chi}_1^+}$
background					
$\gamma\gamma$	6.89	3.31	9.07	13.91	12.99
$\ell^+\ell^-(\gamma)$	0.02	0.16	1.10	2.97	5.39
$q\bar{q}(\gamma)$	0.00	0.00	0.04	0.04	0.04
4f	0.95	1.89	9.72	54.96	97.97
total bkg	7.9 ± 1.1	5.4 ± 0.8	20.0 ± 1.4	71.9 ± 2.1	116.4 ± 2.2
observed	12	8	23	73	112

Table 3: The numbers of expected background events for various Standard Model processes, normalised to the integrated luminosity, and the number of observed events in each ΔM_+ region for category (C). The errors in the total background include only the statistical error of the Monte Carlo samples.

3.2 Detection of neutralinos

To obtain optimal performance, the event sample is divided into two mutually exclusive categories, motivated by the topologies expected for neutralino events.

- (C) $N_{\text{ch}} \leq 4$. Signal events in which $\tilde{\chi}_2^0$ decays into $\tilde{\chi}_1^0\ell^+\ell^-$ tend to fall into this category. Also, when the mass difference between $\tilde{\chi}_2^0$ and $\tilde{\chi}_1^0$ ($\Delta M_0 \equiv m_{\tilde{\chi}_2^0} - m_{\tilde{\chi}_1^0}$) is small, signal events tend to fall into this category independently of the $\tilde{\chi}_2^0$ decay channel.
- (D) $N_{\text{ch}} > 4$. Signal events in which $\tilde{\chi}_2^0$ decays into $\tilde{\chi}_1^0q\bar{q}$ tend to fall into this category for modest and large values of ΔM_0 .

The event topology of $\tilde{\chi}_1^0\tilde{\chi}_2^0$ events depends mainly on the difference between the $\tilde{\chi}_2^0$ and $\tilde{\chi}_1^0$ masses. Separate selection criteria are therefore used in four ΔM_0 regions: (i) $\Delta M_0 \leq 10$ GeV, (ii) $10 < \Delta M_0 \leq 30$ GeV, (iii) $30 < \Delta M_0 \leq 80$ GeV, (iv) $\Delta M_0 > 80$ GeV. In regions (i) and (ii), the main sources of background are two-photon and $\gamma^*Z^{(*)} \rightarrow q\bar{q}\nu\bar{\nu}$ processes. In regions (iii) and (iv), the main sources of background are four-fermion processes (W^+W^- , $We\nu$ and $\gamma^*Z^{(*)}$). The fraction of events falling into category (C) is 10-20% for $\Delta M_0 \geq 20$ GeV but increases to

about 70% when $\Delta M_0 \leq 5$ GeV. The fraction of invisible events due to $\tilde{\chi}_2^0 \rightarrow \tilde{\chi}_1^0 Z^{(*)} \rightarrow \tilde{\chi}_1^0 \nu \bar{\nu}$ decays is 20-30% depending on ΔM_0 .

The selection criteria applied for the low-multiplicity events (category (C)) in regions (i), (ii), (iii) and (iv) are identical to those used in analysis (C) of the chargino search in regions (Ia), (II), (III) and (IV), respectively (see Table 3).

Events falling into category (D) have typically a monojet or a di-jet topology with large missing transverse momentum. The cuts described below are applied for these topologies. They are identical to the ones of Ref. [10] unless otherwise stated.

3.2.1 Analysis (D) ($N_{\text{ch}} > 4$)

To reduce the background from two-photon and $q\bar{q}(\gamma)$ processes, cuts on $|\cos(\theta_{\text{miss}})|$, $E_{\text{fwd}}/E_{\text{vis}}$ and missing transverse momenta are applied. The acoplanarity angle should be large to remove $q\bar{q}(\gamma)$ background events. To ensure the reliability of the measurement of ϕ_{acop} , both jets should have a polar angle θ_j satisfying $|\cos\theta_j| < 0.95$. In region (iv), the ϕ_{acop} cut is loosened with respect to regions (i)–(iii), since the acoplanarity angle of signal events becomes smaller. To compensate for the resulting higher $q\bar{q}(\gamma)$ background, the $E_{\text{fwd}}/E_{\text{vis}}$ cut is tightened.

After these cuts, the remaining background events come predominantly from $\gamma^* Z^{(*)} \rightarrow q\bar{q}\nu\bar{\nu}$, $W^+W^- \rightarrow \ell\nu q\bar{q}'$ and $W e\nu \rightarrow q\bar{q}' e\nu$. Cuts on the visible mass are applied to reduce $W^+W^- \rightarrow \ell\nu q\bar{q}'$ and $W e\nu \rightarrow q\bar{q}' e\nu$ processes. $\gamma^* Z^{(*)} \rightarrow q\bar{q}\nu\bar{\nu}$ background events are removed by a cut on the ratio of the visible mass to the visible energy, which is required to be larger than 0.3 for region (i) and 0.25 for regions (ii) and (iii). In regions (iii) and (iv), $d_{23}^2 \equiv y_{23} E_{\text{vis}}^2 < 30$ GeV² is required to select a clear two-jet topology and to reject $W^+W^- \rightarrow \tau\nu q\bar{q}'$ events. In Figure 1(d) the d_{23}^2 distribution is shown for region (iv) after all the other cuts. The numbers of background events expected from the four different sources, for each ΔM_0 region, are given in Table 4. Typical detection efficiencies for $\tilde{\chi}_2^0 \tilde{\chi}_1^0$ events are 50–65% for $\Delta M_0 > 10$ GeV.

Region	i	ii	iii	iv
	$\Delta M_0 \leq 10$ GeV	$10 \text{ GeV} < \Delta M_0 \leq 30$ GeV	$30 \text{ GeV} < \Delta M_0 \leq 80$ GeV	$\Delta M_0 > 80$ GeV
background				
$\gamma\gamma$	3.06	4.91	1.48	0.00
$\ell^+\ell^-(\gamma)$	0.00	0.07	0.13	0.33
$q\bar{q}(\gamma)$	0.00	0.00	0.00	0.04
4f	0.25	4.62	11.72	39.97
total bkg	3.3 ± 1.1	9.6 ± 1.5	13.3 ± 1.0	40.3 ± 1.2
observed	2	8	14	39

Table 4: The numbers of expected background events for various Standard Model processes, normalised to the integrated luminosity, and the number of observed events in each ΔM_0 region for category (D). The errors in the total background include only the statistical error of the Monte Carlo samples.

4 Systematic uncertainties

Systematic uncertainties on the number of expected signal and background events are estimated in the same manner as in the previous papers [8] and [10] and are only briefly described here.

For the number of expected signal events the uncertainties arise from the measurement of the integrated luminosity (0.5%), Monte-Carlo statistics and interpolation of the efficiencies to arbitrary values of $m_{\tilde{\chi}_1^\pm}$ and $m_{\tilde{\chi}_1^0}$ (2–10%), modelling of the cut variables in the Monte Carlo simulations (4–10%), fragmentation uncertainties in hadronic decays ($< 2\%$) and detector calibration effects ($< 1\%$).

The angular distributions of the chargino and neutralino final-state decay products and their effect on the resulting signal detection efficiencies depend on the details of the parameters of the Constrained MSSM [1]. However, the corresponding variation of the efficiencies is determined to be less than 5% (relative), and this is taken into account in the systematic errors when obtaining the limits. Consequently, the limits are independent of the details of the Constrained MSSM.

For the expected number of background events, the uncertainties are due to Monte Carlo statistics (see Tables 1 to 4), uncertainties in the amount of two-photon background (30%), uncertainties in the simulation of the four-fermion processes (17%), and modelling of the cut variables ($< 7\%$), as determined in Ref. [8].

In addition to effects included in the detector simulation, an efficiency loss of 2.9% (relative) arises from beam-related background in the silicon-tungsten forward calorimeter and in the forward detector which is estimated using random beam crossing events.

5 Results

No evidence for $\tilde{\chi}_1^+ \tilde{\chi}_1^-$ and $\tilde{\chi}_1^0 \tilde{\chi}_2^0$ production is observed. Exclusion regions and limits are determined by using the likelihood ratio method [26], which assigns greater weight to the analysis which has the largest sensitivity. Systematic uncertainties on the efficiencies and on the number of expected background events are taken into account in the cross-section limit calculations according to Ref. [27].

5.1 Limits on the $\tilde{\chi}_1^+ \tilde{\chi}_1^-$ and $\tilde{\chi}_2^0 \tilde{\chi}_1^0$ production cross-sections

Figures 2(a) and (b) show model-independent upper-limits (95% C.L.) on the production cross-sections of $\tilde{\chi}_1^+ \tilde{\chi}_1^-$ and $\tilde{\chi}_2^0 \tilde{\chi}_1^0$, respectively. These are obtained assuming the specific decay mode $\tilde{\chi}_1^\pm \rightarrow \tilde{\chi}_1^0 W^{(*)\pm}$ for $\tilde{\chi}_1^+ \tilde{\chi}_1^-$, and $\tilde{\chi}_2^0 \rightarrow \tilde{\chi}_1^0 Z^{(*)}$ for $\tilde{\chi}_1^0 \tilde{\chi}_2^0$ production. The results from the $\sqrt{s}=183$ GeV [10] analysis are also included in the limit calculation ⁶.

If the cross-section for $\tilde{\chi}_1^+ \tilde{\chi}_1^-$ is larger than 0.75 pb and ΔM_+ is between 5 GeV and about 80 GeV, $m_{\tilde{\chi}_1^+}$ is excluded at the 95% C.L. up to the kinematic limit. If the cross-section for $\tilde{\chi}_2^0 \tilde{\chi}_1^0$ is larger than 0.95 pb and ΔM_0 is greater than 7 GeV, $m_{\tilde{\chi}_2^0}$ is excluded up to the kinematic limit at 95% C.L.

⁶ In calculating limits, cross-sections at different \sqrt{s} were estimated by weighting by $\bar{\beta}/s$, where $\bar{\beta}$ is $p_{\tilde{\chi}_1^\pm}/E_{\text{beam}}$ for $\tilde{\chi}_1^+ \tilde{\chi}_1^-$ production or $p_{\tilde{\chi}_2^0}/E_{\text{beam}} = p_{\tilde{\chi}_1^0}/E_{\text{beam}}$ for $\tilde{\chi}_2^0 \tilde{\chi}_1^0$ production.

5.2 Limits in the MSSM parameter space

The phenomenology of the gaugino-higgsino sector of the MSSM is mostly determined by the following parameters: the SU(2) gaugino mass parameter at the weak scale (M_2), the mixing parameter of the two Higgs doublet fields (μ) and the ratio of the vacuum expectation values of the two Higgs doublets ($\tan\beta$). Assuming sfermions [3] and SUSY Higgs [28] sufficiently heavy not to intervene in the decay channels, these three parameters are sufficient to describe the chargino and neutralino sectors completely. Within the Constrained MSSM [1], a large value of the common scalar mass, m_0 (e.g., $m_0 = 500$ GeV) leads to heavy sfermions and therefore to a negligible suppression of the cross-section due to interference with t -channel sneutrino exchange. Chargino decays would then proceed predominantly via a virtual or real W. On the other hand, a light m_0 results in a low value of the mass of the sneutrino, enhancing the contribution of the t -channel exchange diagrams that have destructive interference with s -channel diagrams, thus reducing the cross-section for chargino pair production. Small values of m_0 also enhance the leptonic branching ratio of charginos.

From the input parameters M_2 , μ , $\tan\beta$, m_0 and A (the trilinear Higgs coupling), masses, production cross-sections and branching fractions are calculated according to the Constrained MSSM [1, 2, 4, 5]. For each set of input parameters, the total numbers of $\tilde{\chi}_1^+\tilde{\chi}_1^-$, $\tilde{\chi}_2^0\tilde{\chi}_1^0$, $\tilde{\chi}_3^0\tilde{\chi}_1^0$ and $\tilde{\chi}_2^0\tilde{\chi}_2^0$ events expected to be observed are calculated using the integrated luminosity, the cross-sections, the branching fractions, and the detection efficiencies (which depend upon the masses of the chargino, the lightest neutralino and next-to-lightest neutralino). Contributions from channels such as $\tilde{\chi}_1^0\tilde{\chi}_4^0$, $\tilde{\chi}_2^0\tilde{\chi}_4^0$, etc ... are not included. The $\tilde{\chi}_3^0\tilde{\chi}_1^0$ channel is similar to the $\tilde{\chi}_2^0\tilde{\chi}_1^0$ channel, and cascade decays through $\tilde{\chi}_2^0$ are taken into account. The relative importance of each of the analyses (A)–(D) changes with the leptonic or hadronic branching ratios, and the likelihood ratio method [26] is used to optimally weight each analysis depending on these branching ratios.

Results are presented for two cases: (i) $m_0 = 500$ GeV (i.e., heavy sfermions), and (ii) the value of m_0 that gives the smallest total numbers of expected chargino and neutralino events taking into account cross-sections, branching ratios, and detection efficiencies for each set of values of M_2 , μ and $\tan\beta$. This latter value of m_0 leads to the most conservative limit at that point, so that the resulting limits are valid for all m_0 . In searching for this value of m_0 , only those values are considered that are compatible with the current limits on the sneutrino mass ($m_{\tilde{\nu}_L} > 43$ GeV [29]), and upper limits on the cross-section for slepton pair production, particularly right-handed smuon and selectron pair production [3]. Particular attention is paid to the region of values of m_0 leading to the mass condition $m_{\tilde{\nu}} \approx m_{\tilde{\chi}_1^\pm}$ by taking finer steps in the value of m_0 . Note that we assume the stau mixing angle to be zero, and the added complication of possible enhanced decays to third-generation particles at large values of $\tan\beta$ because of stau mixing is ignored. When $m_{\tilde{\nu}} \leq m_{\tilde{\chi}_1^\pm}$, resulting in a topology of acoplanar leptons and missing momentum, the upper limits on the cross-section for the two-body chargino decay from Ref. [3] are used, while for $m_{\tilde{\nu}} > m_{\tilde{\chi}_1^\pm}$ the three-body decays are dominant. Single photon topologies from $\tilde{\chi}_2^0\tilde{\chi}_1^0$ production and acoplanar photons with missing energy topologies from $\tilde{\chi}_2^0\tilde{\chi}_2^0$ with photonic decay $\tilde{\chi}_2^0 \rightarrow \tilde{\chi}_1^0\gamma$ are taken into account using the 95% C.L. cross-section upper limits on these topologies from OPAL results [30]. In both of these cases, if the relevant product of cross-section and branching ratio for a particular set of MSSM parameters is greater than the measured 95% C.L. upper limit presented in that paper, then that set of parameters is considered to be excluded.

The following regions of the Constrained MSSM parameters are scanned: $0 \leq M_2 \leq 2000$ GeV, $|\mu| \leq 500$ GeV, and $A = \pm M_2, \pm m_0$ and 0. The typical scan step is 0.2 GeV. Extensions beyond the scanned range have negligible effect on the quoted limits. The choice of A values is related to various scenarios of stop mixing, influencing the Higgs sector but having essentially no effect on the gaugino sector. No significant dependence on A is observed. Figure 3 shows the resulting exclusion regions in the (M_2, μ) plane for $\tan \beta = 1.5$ and 35 with $m_0 \geq 500$ GeV and for all m_0 .

The restrictions on the Constrained MSSM parameter space presented here can be transformed into exclusion regions in the $(m_{\tilde{\chi}_1^\pm}, m_{\tilde{\chi}_1^0})$ or $(m_{\tilde{\chi}_2^0}, m_{\tilde{\chi}_1^0})$ plane. A given mass pair is excluded only if all considered Constrained MSSM parameters in the scan which lead to that same mass pair are excluded at the 95% C.L. The $\tilde{\chi}_1^\pm$ mass limits are summarised in Table 5. In the $(m_{\tilde{\chi}_1^\pm}, m_{\tilde{\chi}_1^0})$ plane, Figures 4(a) and (b) show the corresponding 95% C.L. exclusion regions for $\tan \beta = 1.5$ and 35. Figures 4(c) and (d) show the corresponding 95% C.L. exclusion regions in the $(m_{\tilde{\chi}_2^0}, m_{\tilde{\chi}_1^0})$ plane, for $\tan \beta = 1.5$ and 35. Mass limits on $\tilde{\chi}_1^0, \tilde{\chi}_2^0,$ and $\tilde{\chi}_3^0$ are summarised in Table 6.

		$\tan \beta = 1.5$	$\tan \beta = 35$
$m_0 \geq 500$ GeV	$\Delta M_+ \geq 5$ GeV	$m_{\tilde{\chi}_1^+} > 93.6$ GeV	$m_{\tilde{\chi}_1^+} > 94.1$ GeV
All m_0 (see text)	$\Delta M_+ \geq 5$ GeV	$m_{\tilde{\chi}_1^+} > 78.0$ GeV	$m_{\tilde{\chi}_1^+} > 71.7$ GeV

Table 5: Lower limits at 95% C.L. obtained on the lightest chargino mass.

		$\tan \beta = 1.5$	$\tan \beta = 35$
$m_0 \geq 500$ GeV	No ΔM_0 restriction	$m_{\tilde{\chi}_1^0} > 40.2$ GeV	$m_{\tilde{\chi}_1^0} > 48.5$ GeV
	$\Delta M_0 \geq 10$ GeV	$m_{\tilde{\chi}_2^0} > 67.8$ GeV	$m_{\tilde{\chi}_2^0} > 94.3$ GeV
		$m_{\tilde{\chi}_3^0} > 106.0$ GeV	$m_{\tilde{\chi}_3^0} > 124.0$ GeV
All m_0 (see text)	No ΔM_0 restriction	$m_{\tilde{\chi}_1^0} > 34.1$ GeV	$m_{\tilde{\chi}_1^0} > 38.9$ GeV
	$\Delta M_0 \geq 10$ GeV	$m_{\tilde{\chi}_2^0} > 55.9$ GeV	$m_{\tilde{\chi}_2^0} > 86.2$ GeV
		$m_{\tilde{\chi}_3^0} > 106.6$ GeV	$m_{\tilde{\chi}_3^0} > 134.3$ GeV

Table 6: Lower limits at 95% C.L. obtained on $m_{\tilde{\chi}_1^0}, m_{\tilde{\chi}_2^0},$ and $m_{\tilde{\chi}_3^0}$.

Figure 5 shows the dependence of the mass limits on the value of $\tan \beta$. Of particular interest is the absolute lower limit, in the framework of the Constrained MSSM, on the mass of the lightest neutralino of $m_{\tilde{\chi}_1^0} > 32.8$ GeV (31.6 GeV) at 95% C.L. for $m_0 \geq 500$ GeV (all m_0). This has implications for direct searches for the lightest neutralino as a candidate for dark matter [31]. Since the formulae for couplings and masses in the gaugino sector are symmetric in $\tan \beta$ and $1/\tan \beta$, these results also hold for $\tan \beta < 1$.

6 Summary and Conclusion

A data sample corresponding to an integrated luminosity of 182.1 pb^{-1} at $\sqrt{s} = 188.6$ GeV, collected with the OPAL detector, has been analysed to search for pair-production of charginos ($\tilde{\chi}_1^+ \tilde{\chi}_1^-$) and neutralinos ($\tilde{\chi}_2^0 \tilde{\chi}_1^0$) predicted by supersymmetric theories. Decays of $\tilde{\chi}_1^\pm$ into $\tilde{\chi}_1^0 \ell^\pm \nu$ or $\tilde{\chi}_1^0 q \bar{q}'$ and decays of $\tilde{\chi}_2^0$ into $\tilde{\chi}_1^0 \nu \bar{\nu}, \tilde{\chi}_1^0 \ell^+ \ell^-$ or $\tilde{\chi}_1^0 q \bar{q}$ are looked for. No evidence for such events

has been observed. The exclusion limits on $\tilde{\chi}_1^\pm$ and $\tilde{\chi}_j^0$ production are significantly higher with respect to the results obtained at lower centre-of-mass energies.

Exclusion regions valid at the 95% confidence level have been derived in the framework of the Constrained MSSM, in which only three parameters (M_2 , μ and $\tan\beta$) are necessary to describe the chargino and neutralino sectors. These restrictions in parameter space have been transformed into mass limits valid at the 95% confidence level. Assuming $m_{\tilde{\chi}_1^\pm} - m_{\tilde{\chi}_1^0} \geq 5$ GeV, the lower mass limit of the chargino is 93.6 GeV for $\tan\beta = 1.5$ and 94.1 GeV for $\tan\beta = 35$ for the case of a large universal scalar mass ($m_0 \geq 500$ GeV); for all m_0 , the mass limit is 78.0 GeV for $\tan\beta = 1.5$ and 71.7 GeV for $\tan\beta = 35$. The lower mass limit for the lightest neutralino is 32.8 GeV for the case of $m_0 \geq 500$ GeV and 31.6 GeV for all m_0 . This latter result has implications for searches for the lightest neutralino as a dark matter candidate.

Acknowledgements

We particularly wish to thank the SL Division for the efficient operation of the LEP accelerator at all energies and for their continuing close cooperation with our experimental group. We thank our colleagues from CEA, DAPNIA/SPP, CE-Saclay for their efforts over the years on the time-of-flight and trigger systems which we continue to use. In addition to the support staff at our own institutions we are pleased to acknowledge the

Department of Energy, USA,

National Science Foundation, USA,

Particle Physics and Astronomy Research Council, UK,

Natural Sciences and Engineering Research Council, Canada,

Israel Science Foundation, administered by the Israel Academy of Science and Humanities,

Minerva Gesellschaft,

Benoziyo Center for High Energy Physics,

Japanese Ministry of Education, Science and Culture (the Monbusho) and a grant under the Monbusho International Science Research Program,

Japanese Society for the Promotion of Science (JSPS),

German Israeli Bi-national Science Foundation (GIF),

Bundesministerium für Bildung, Wissenschaft, Forschung und Technologie, Germany,

National Research Council of Canada,

Research Corporation, USA,

Hungarian Foundation for Scientific Research, OTKA T-029328, T023793 and OTKA F-023259.

References

- [1] H.P. Nilles, Phys. Rep. **110** (1984) 1;
H.E. Haber and G.L. Kane, Phys. Rep. **117** (1985) 75.
- [2] M. Chen, C. Dionisi, M. Martinez and X. Tata, Phys. Rep. **159** (1988) 201;
A. Bartl, H. Fraas and W. Majerotto, Z. Phys. **C30** (1986) 441;
A. Bartl, H. Fraas and W. Majerotto, Z. Phys. **C41** (1988) 475;

- A. Bartl, H. Fraas, W. Majerotto and B. Mösslacher, Z. Phys. **C55** (1992) 257;
 J.L. Feng and M.J. Strassler, Phys. Rev. **D51** (1995) 4661.
- [3] OPAL Collab., G. Abbiendi *et al.*, ‘Search for Anomalous Production of Acoplanar Di-Lepton Events in e^+e^- Collisions at $\sqrt{s} = 183$ and 189 GeV’, CERN-EP/xxxx, To be submitted to Eur. Phys. J. **C**.
- [4] A. Bartl, H. Fraas and W. Majerotto, Nucl. Phys. **B278** (1986) 1;
 S. Ambrosanio and B. Mele, Phys. Rev. **D52** (1995) 3900.
- [5] M. Carena, J.R. Espinosa, M. Quiros and C.E.M. Wagner, Phys. Lett. **B355** (1995) 209.
- [6] ALEPH Collab., D. Buskulic *et al.*, Phys. Lett. **B373** (1996) 246;
 DELPHI Collab., P. Abreu *et al.*, Phys. Lett. **B382** (1996) 323;
 L3 Collab., M. Acciarri *et al.*, Phys. Lett. **B377** (1996) 289;
 OPAL Collab., G. Alexander *et al.*, Phys. Lett. **B377** (1996) 181.
- [7] OPAL Collab., K. Ackerstaff *et al.*, Phys. Lett. **B389** (1996) 616.
- [8] OPAL Collab., K. Ackerstaff *et al.*, Eur. Phys. J. **C2** (1998) 213.
- [9] ALEPH Collab., R. Barate *et al.*, Eur. Phys. J. **C2** (1998) 417;
 DELPHI Collab., P. Abreu *et al.*, Eur. Phys. J. **C1** (1998) 1;
 L3 Collab., M. Acciarri *et al.*, Eur. Phys. J. **C4** (1998) 207.
- [10] OPAL Collab., G. Abbiendi *et al.*, Eur. Phys. J. **C8** (1999) 255.
- [11] DELPHI Collab., P. Abreu *et al.*, Phys. Lett. **B466** (1999) 75;
 ALEPH Collab., R. Barate *et al.*, CERN 99-014, Submitted to Eur. Phys. J. **C**.
- [12] OPAL Collab., K. Ahmet *et al.*, Nucl. Instr. Meth. **A305** (1991) 275;
 S. Anderson *et al.*, Nucl. Instr. Meth. **A403** (1998) 326;
 B.E. Anderson *et al.*, IEEE Trans. on Nucl. Science **41** (1994) 845.
- [13] G. Aguillion *et al.*, Nucl. Instr. Meth. **A417** (1998) 266.
- [14] C. Dionisi *et al.*, in ‘Physics at LEP2’, eds. G. Altarelli, T. Sjöstrand and F. Zwirner, CERN 96-01, vol.2, 337.
- [15] T. Sjöstrand, Comp. Phys. Comm. **82** (1994) 74;
 T. Sjöstrand, Lund University report LU TP 95-20.
- [16] S. Katsanevas and P. Morawitz, Comp. Phys. Comm. **112** (1998) 227.
- [17] R. Engel, Z. Phys. **C66** (1995) 203;
 R. Engel and J. Ranft, Phys. Rev. **D54** (1996) 4246.
- [18] G. Marchesini *et al.*, Comp. Phys. Comm. **67** (1992) 465.
- [19] J.A.M. Vermaseren, Nucl. Phys. **B229** (1983) 347.
- [20] J. Fujimoto *et al.*, Comp. Phys. Comm. **100** (1997) 128.
- [21] S. Jadach, B.F.L. Ward and Z. Wąs, Comp. Phys. Comm. **79** (1994) 503.

- [22] S. Jadach, W. Placzek and B.F.L. Ward, in ‘Physics at LEP2’, eds. G. Altarelli, T. Sjöstrand and F. Zwirner, CERN 96-01, vol. 2, 286.
- [23] J. Allison *et al.*, Nucl. Instr. Meth. **A317** (1992) 47.
- [24] R.M. Barnett *et al.* (Particle Data Group), Phys. Rev. **D54** (1996) 166 Eq. (28.40).
- [25] S. Catani *et al.*, Phys. Lett. **B269** (1991) 432.
- [26] A.G. Frodesen, O. Skeggestad, and H. Tofte, ‘Probability and Statistics in Particle Physics’, Universitetsforlaget, 1979, ISBN 82-00-01-01906-3;
S.L. Meyer, ‘Data Analysis for Scientists and Engineers’, John Wiley and Sons, 1975, ISBN 0-471-59995-6.
- [27] R.D. Cousins and V.L. Highland, Nucl. Instr. Meth. **A320** (1992) 331.
- [28] OPAL Collab., G. Abbiendi *et al.*, ‘Search for Neutral Higgs Bosons in e^+e^- Collisions at $\sqrt{s} \approx 189$ GeV’, CERN-EP/99-096, Submitted to Eur. Phys. J. **C**.
- [29] C. Caso *et al.* (Particle Data Group), Eur. Phys. J. **C3** (1998) 760.
- [30] OPAL Collab., G. Abbiendi *et al.*, Eur. Phys. J. **C8** (1999) 23.
- [31] P.F. Smith and J.D. Lewin, Phys. Rep. **187** (1990) 203.

OPAL

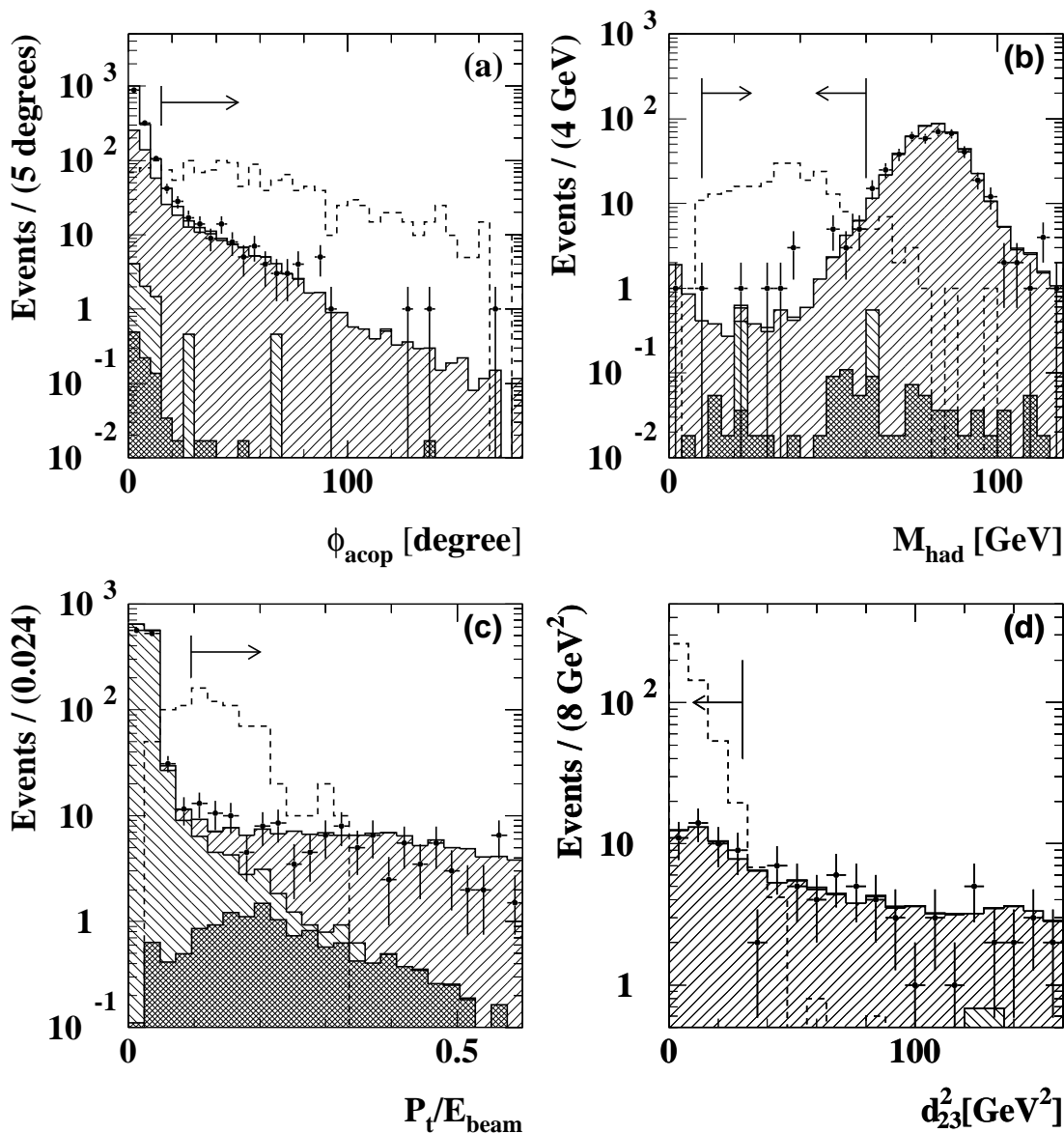


Figure 1: Distributions of some essential observables used to select chargino and neutralino events: (a) acoplanarity angle in analysis (A), (b) invariant mass of the event calculated excluding the highest momentum isolated lepton in analysis (B), (c) ratio of transverse momentum to beam energy, P_t/E_b , in analysis (C), and (d) d_{23}^2 in analysis (D). The data are shown with error bars and the distributions from the background processes are shown as filled histograms: dilepton events (double hatched area), two-photon processes (negative slope hatching area), four-fermion processes including W-pair events (positive slope hatching area), and multihadronic events (open area). The arrows, pointing into the accepted regions, show where the analysis cuts are applied. In Figures (a)-(c) the dashed line shows the prediction for a chargino signal with $m_{\tilde{\chi}_1^+} = 94$ GeV and $m_{\tilde{\chi}_1^0} = 47$ GeV. In Figure (d) the dashed line shows the prediction for a neutralino signal with $m_{\tilde{\chi}_2^0} = 145$ GeV and $m_{\tilde{\chi}_1^0} = 35$ GeV. The normalisations of the signal histograms are arbitrary.

OPAL

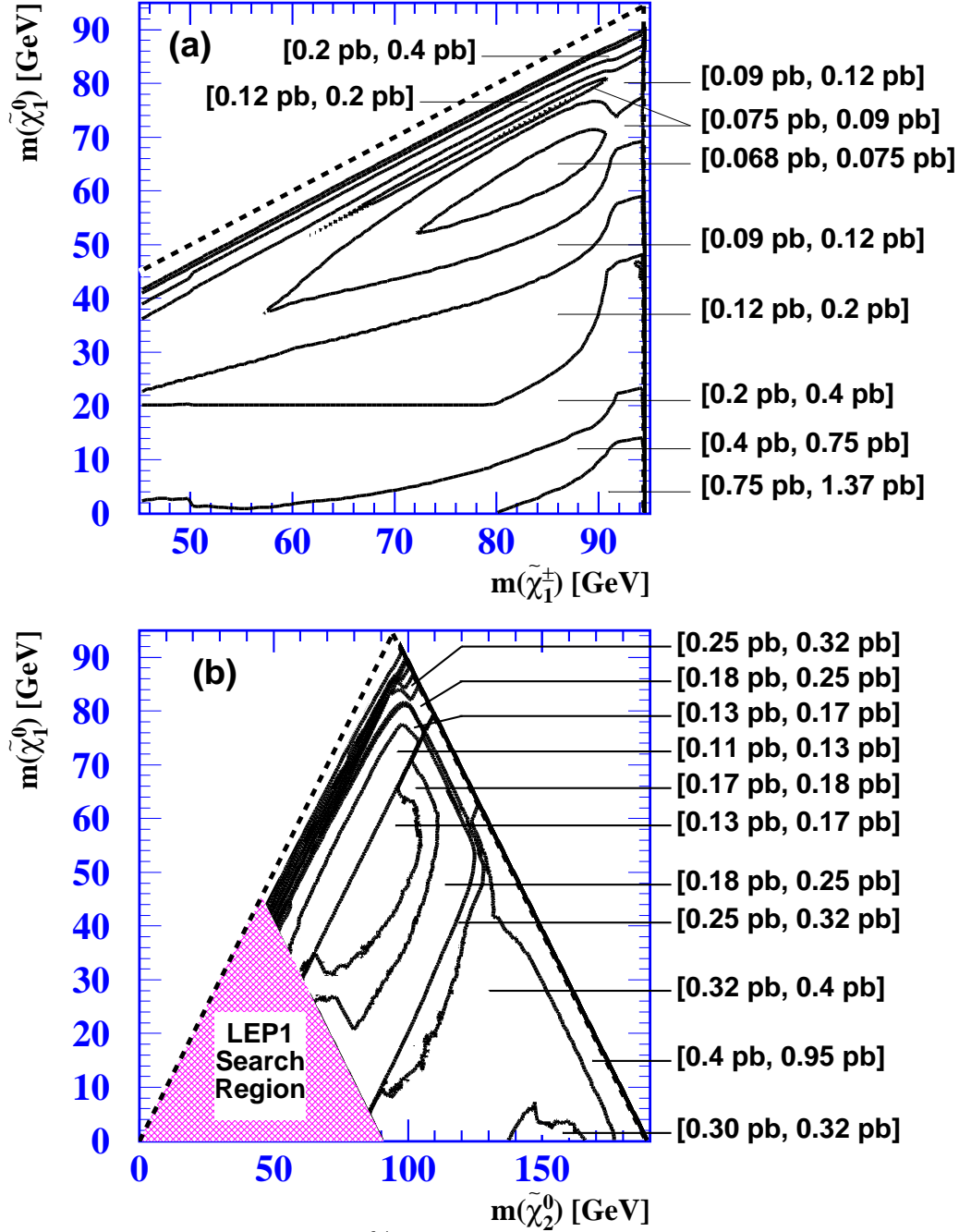


Figure 2: Contour plots of the 95% C.L. upper-limits on the production cross-sections at $\sqrt{s} = 189$ GeV (a) $\sigma_{\tilde{\chi}_1^+ \tilde{\chi}_1^-}$ for $e^+e^- \rightarrow \tilde{\chi}_1^+ \tilde{\chi}_1^-$ and (b) $\sigma_{\tilde{\chi}_2^0 \tilde{\chi}_1^0}$ for $e^+e^- \rightarrow \tilde{\chi}_1^0 \tilde{\chi}_2^0$. The $\tilde{\chi}_1^+$ is assumed to decay only into $\tilde{\chi}_1^0 W^{(*)\pm}$, and the $\tilde{\chi}_2^0$ is assumed to decay only into $\tilde{\chi}_1^0 Z^{(*)}$. The cross-hatched region, for which $m_{\tilde{\chi}_1^0} + m_{\tilde{\chi}_2^0} < m_Z$, is covered by searches at LEP1, which set upper-limits on $\sigma_{\tilde{\chi}_2^0 \tilde{\chi}_1^0}$ of order 5 pb, and is not considered in this analysis. The kinematical boundaries for $\tilde{\chi}_1^+ \tilde{\chi}_1^-$ and $\tilde{\chi}_1^0 \tilde{\chi}_2^0$ are shown as dashed lines. If $\sigma_{\tilde{\chi}_1^+ \tilde{\chi}_1^-}$ is smaller than 0.068 pb, there is no exclusion region in the $(m_{\tilde{\chi}_1^+}, m_{\tilde{\chi}_1^0})$ plane. If $\sigma_{\tilde{\chi}_1^+ \tilde{\chi}_1^-}$ is between 0.068 and 0.075 pb a small region is excluded around $m_{\tilde{\chi}_1^+} = 85$ GeV and $m_{\tilde{\chi}_1^0} = 65$ GeV. Similarly, if $\sigma_{\tilde{\chi}_2^0 \tilde{\chi}_1^0}$ is smaller than 0.11 pb no region can be excluded in the $(m_{\tilde{\chi}_2^0}, m_{\tilde{\chi}_1^0})$ plane. If $\sigma_{\tilde{\chi}_2^0 \tilde{\chi}_1^0}$ is between 0.11 and 0.13 pb a small region is excluded around $\Delta M_0 \equiv m_{\tilde{\chi}_2^0} - m_{\tilde{\chi}_1^0} = 25$ GeV.

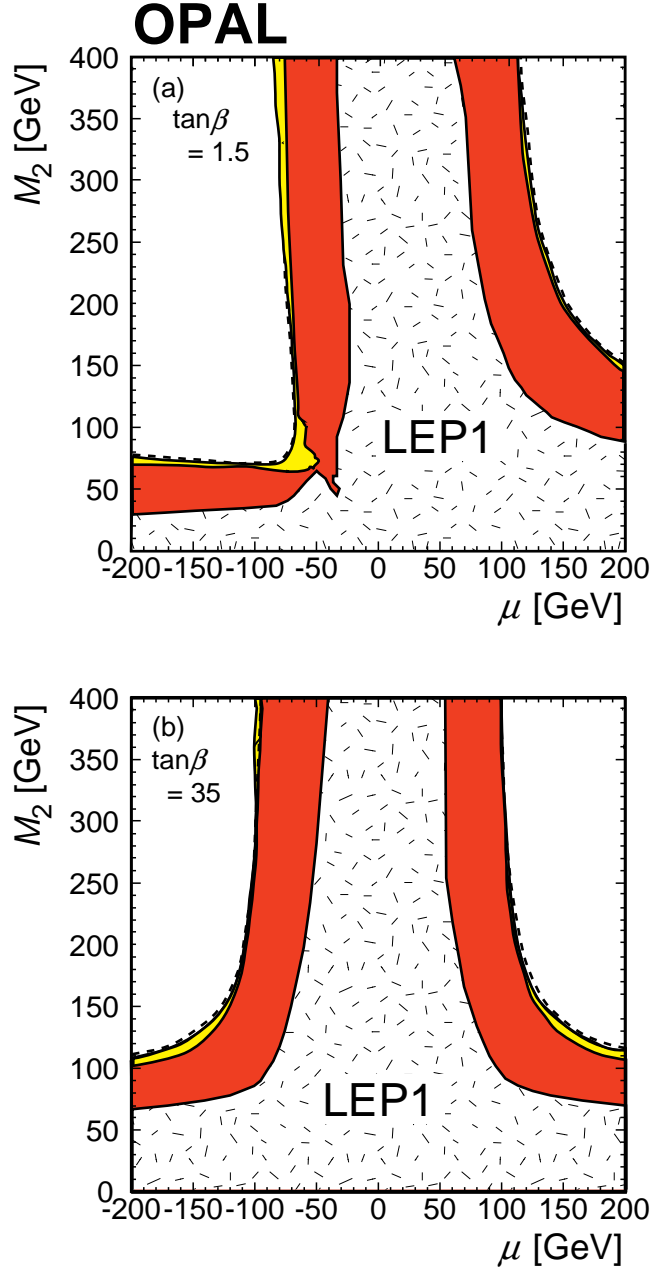


Figure 3: Exclusion regions at 95% C.L. in the μ - M_2 plane within the framework of the Constrained MSSM for (a) $\tan\beta = 1.5$ and (b) $\tan\beta = 35$. The speckled areas show the regions excluded by LEP1 data, and the shaded areas the additional exclusion regions using the data from $\sqrt{s} = 183$ and 189 GeV. The dark-shaded regions are valid for all values of m_0 , and the light-shaded regions are the additional excluded parameters if $m_0 \geq 500$ GeV (i.e., heavy scalar leptons). The kinematical boundary at $\sqrt{s} = 189$ GeV for $\tilde{\chi}_1^+ \tilde{\chi}_1^-$ production is shown by dashed lines.

OPAL

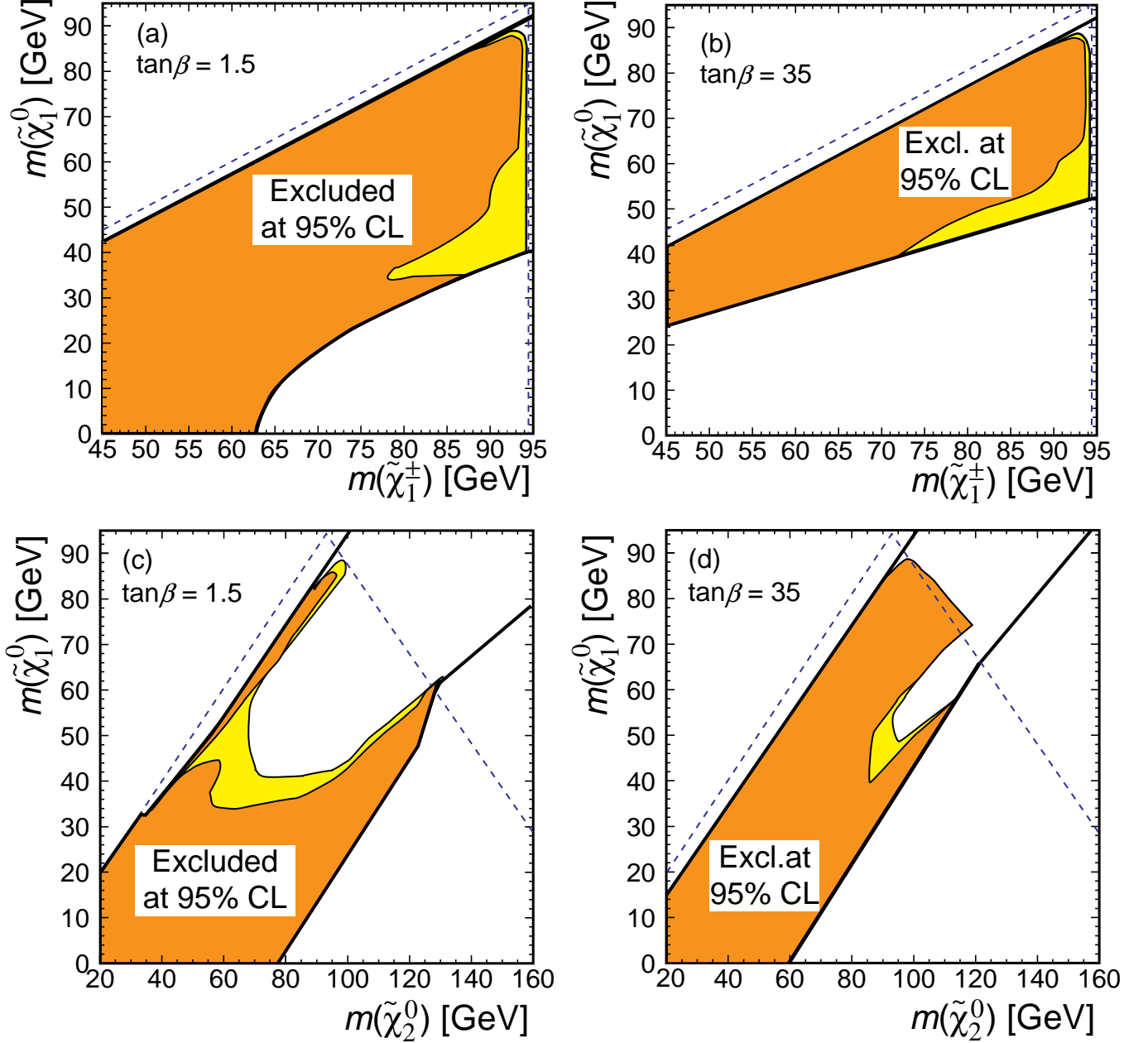


Figure 4: The 95% C.L. excluded regions in the $(m_{\tilde{\chi}_1^\pm}, m_{\tilde{\chi}_1^0})$ plane within the framework of the Constrained MSSM for the case of any value of m_0 (dark-shaded regions) and $m_0 \geq 500$ GeV (extending to light-shaded regions) for (a) $\tan\beta = 1.5$ and (b) $\tan\beta = 35$. The thick solid lines represent the theoretical bounds of the Constrained MSSM parameter space. The kinematical boundaries for production and decay at $\sqrt{s} = 189$ GeV are shown by dashed lines. Similar plots for neutralino masses are shown in (c) for $\tan\beta = 1.5$ and (d) for $\tan\beta = 35$.

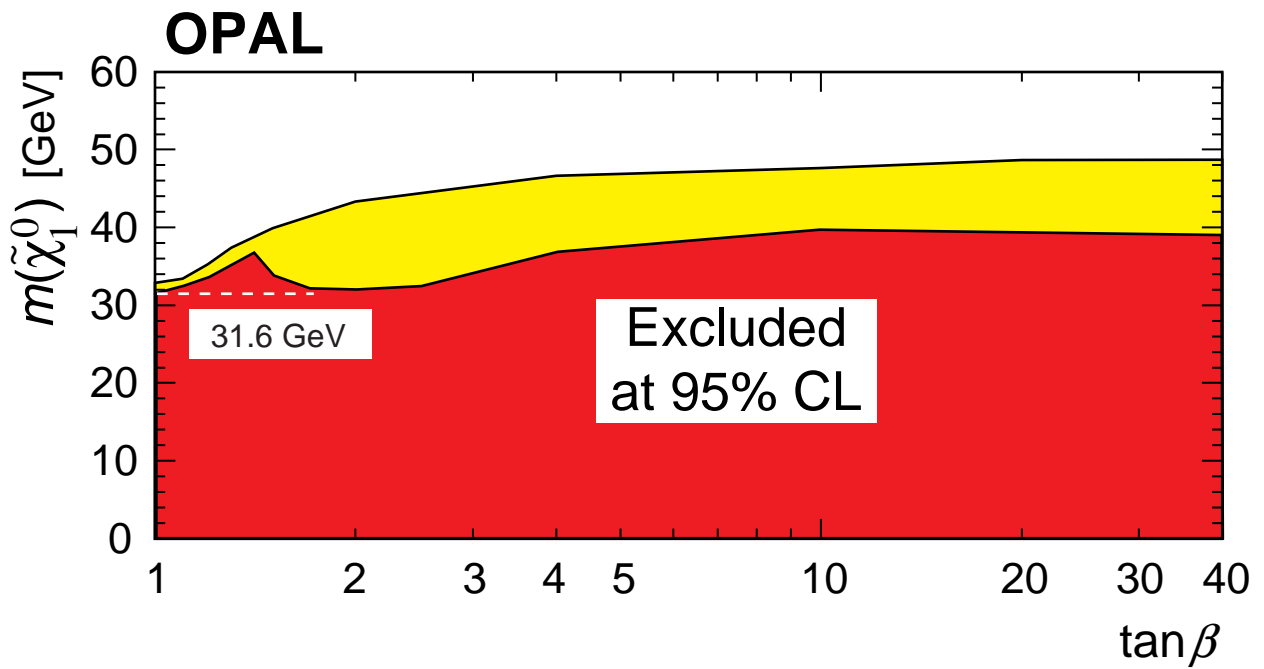


Figure 5: The 95% C.L. mass limit on the lightest neutralino $\tilde{\chi}_1^0$ as a function of $\tan\beta$ within the framework of the Constrained MSSM. Exclusion regions for all m_0 values (dark-shaded region) and $m_0 \geq 500$ GeV (extending to the light-shaded region).